coatings

MDPI

Article

A New Process for Efficient Non-Destructive Metal-Activated Composite Plating of Ni-P-Al_2O_3 on Titanium Base and Its Performance Research

Kaifang Cui [1,2,†], Jin Gao [1,†], Siqi Li [1,†], Xue Leng [3], Liang Zhong [1,*] and Rongming Qiang [1]

[1] School of Manufacturing Science and Engineering, Southwest University of Science and Technology, Mianyang 621010, China; cuikaifang@swust.edu.cn (K.C.); gaojin@mails.swust.edu.cn (J.G.); lisiqi@swust.edu.cn (S.L.); qiangrongming@mails.swust.edu.cn (R.Q.)
[2] The Engineering Technology Center, Southwest University of Science and Technology, Mianyang 621000, China
[3] Sichuan Electronic Machinery Vocational and Technical College, Mianyang 621052, China; lengxue@scemvtc.edu.cn
* Correspondence: zhongliang@swust.edu.cn
† These authors contributed equally to this work.

Abstract: A new high efficient and non-destructive mental activation process of electroless composite plating was proposed. The process utilized electromagnetic induction equipment to heat the titanium alloy substrate and used its energy to complete the activation process, which could successfully attach the nickel nanoparticles firmly to the surface of the titanium alloy; at the same time, the process pre-activated Al_2O_3 nanoparticles and added the activated nanoparticles to the plating solution. In the process of plating, the activated titanium substrate was used as the catalytic center of electroless nickel plating (ENP) for electroless composite plating. The new activation process avoided complicated traditional processes such as acid etching and zinc dipping. Such traditional processes require huge doses of chemicals, including various strong acids, so improper waste liquid treatment will cause harm to the environment. The important parameters of the process were optimized by orthogonal experiments. A scanning electron microscope (SEM), an X-ray photoelectron spectroscopy (XPS), an energy dispersive spectrometer (EDS), thermal shock experiments and friction and wear experiments were used to characterize and analyze the surface morphology, composition, binding force and friction coefficient of the coating, and analyze the coating quality by measuring the plating rate and the thickness of the coating. The results showed that the rate of electroless composite plating increased with the increase in Al_2O_3 nanoparticle concentration. When the concentration of Al_2O_3 nanoparticles reached 1.5 g/L, the ENP rate decreased with the increase in Al_2O_3 nanoparticle concentration. The adhesion of the sample was evaluated by the scratch test, which showed that the binding grade of the sample was 0, and the Vickers hardness was 688.5 HV. Results showed that the coating produced by this new process has excellent performance. Therefore, the process is an environmentally friendly and fast activation composite plating process.

Keywords: electroless composite plating; titanium alloy; Al_2O_3 nanoparticles; high efficient and non-destructive; metal activation

Citation: Cui, K.; Gao, J.; Li, S.; Leng, X.; Zhong, L.; Qiang, R. A New Process for Efficient Non-Destructive Metal-Activated Composite Plating of Ni-P-Al_2O_3 on Titanium Base and Its Performance Research. *Coatings* **2024**, *14*, 1203. https://doi.org/10.3390/coatings14091203

Academic Editor: Vincent Ji

Received: 11 August 2024
Revised: 9 September 2024
Accepted: 16 September 2024
Published: 19 September 2024

1. Introduction

With the development of the aerospace industry, the materials required by this industry must be high specific strength materials. Titanium alloy is the most outstanding in performance and widely used materials among high specific strength materials. However, the disadvantages of low surface hardness, poor tribological performance and easy oxidation at high temperatures limit the application range of titanium alloys [1–5].

The commonly used treatment processes to improve the surface performance of materials include electroplating [6], spraying organic coatings [7], electroless plating [8,9],

vapor deposition [10], micro-arc oxidation [11] and plasma spray [12], etc. Among them, electroless plating is widely used due to its low cost and good coating quality. The addition of the second phase to electroless plating is electroless composite plating. And the addition of nanoparticles to electroless composite plating is a low-cost and performance-improving method because they can form more uniform and stronger grain boundaries in the material. Therefore, the nanoparticles can enhance the hardness and strength of the material, and characterize their own properties on the coating. In an electroless composite plating process, the substrate is usually pre-treated accordingly, and the commonly used metal surface pre-treatment today is zinc dipping, which means that, after removing the surface oxidate layer, a zinc layer is formed on the surface of the substrate by zinc dipping, achieving the purpose of separating the substrate from air contact, and, at the same time, playing the role of activation [13–15]. The process is not only cumbersome to operate but also uses a large amount of corrosive chemicals; this is too costly and has a certain impact on the environment. Therefore, this paper proposes a new high efficient and non-destructive activation process of electroless composite plating (Figure 1), in which a uniformly distributed nickel activation layer is prepared on the surface of a titanium alloy without using strong corrosive chemicals. Then, Al_2O_3 nanoparticles are pre-activated to provide more particle attachment sites for electroless composite plating and, finally, a composite Ni-P/Al_2O_3 layer with strong binding force is obtained through electroless composite plating [16–19].

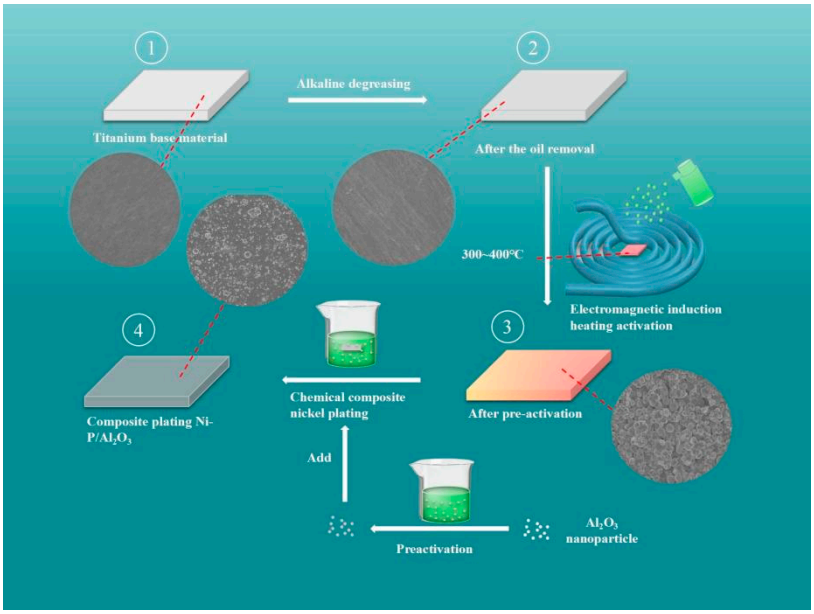

Figure 1. Flow diagram of the electroless composite plating Ni-P/Al_2O_3 process.

In order to give titanium alloys wider application prospects, many scholars have conducted a lot of research on improving the performance of titanium alloys. For example, the Ni-B coating prepared by Jia on the surface of a titanium alloy had high hardness and low wear rates [20]. Cao prepared ultrasonic electroless plating of Ni-P on titanium alloy pre-treated two times with zinc dipping and alkaline pre-plating, and then conducted heat treatment at different temperatures. The experiment showed that the abrasion resistance was increased accordingly [21]. Cui proposed a new activation method for the pre-treatment of electroless plating to study the relationship between the amount of activator and the coating structure, and determine the optimum amount of the activator [22]. Long prepared Ni-W-Cr-P quaternary alloy coatings on the surface of a titanium-base alloy and studied the performance of the coating. The results showed that the microhardness and corrosion resistance of the coatings changed accordingly due to the different organizations after annealing [23]. Zhong prepared a composite coating, added PTFE nanoparticles and

analyzed the friction and wear performance of the samples. The results showed that the friction coefficient of the prepared coating was reduced and the lubricating performance of the coating was improved [24]. R. Uma Rani prepared a super black coating on the surface of titanium alloys with high optical properties to investigate the blackening process for electroless nickel plating. The coating had good adhesion, homogeneity and stability in harsh environments [25]. Alhamad Rusul Khalid adopted the method of electroless nickel plating and deposited Ni-P-TiC nanocomposite coating on alumina substrate, which enhanced corrosion resistance and had a low friction coefficient [26].

2. Materials and Methods

2.1. Materials

Ti6Al4V board was selected as the experimental material substrate, with dimensions of 10 mm × 10 mm × 1 mm. The main chemicals were NaOH, Na_2CO_3, $Na_3PO_4{\cdot}12H_2O$, $Ni_2SO_4{\cdot}6H_2O$, $NaH_2PO_2{\cdot}H_2O$, $CH_3COONa{\cdot}3H_2O$ and $C_6H_5Na_3O_7{\cdot}2H_2O$.

2.2. Pre-Treatment

2.2.1. Sample Substrate Etching

The titanium alloy substrate was immersed in the degreasing solution (composition as shown in Table 1) for 15 min, and then placed in deionized water for ultrasonic cleaning for 5 min.

Table 1. Degreasing solution formulations.

Reagent	Concentration
NaOH	25~40 g/L
Na_2CO_3	40~45 g/L
Na_3PO_4	40~45 g/L

2.2.2. Substrate Activation

The cleaned substrate was soaked in the activation solution (shown in Table 2) for 5 min, and then the sample was placed horizontally in the electromagnetic induction heating coil for heating. When the heating temperature reached above 200 °C, the nickel element was generated on the surface of the substrate, as shown in reaction Equation (1), and an atomizer was used to spray activation solution on its surface. In order to avoid the sudden drop in substrate surface temperature caused by the sprayed activation solution, the surface temperature of the substrate should be higher than 200 °C. Also, the distance between the atomizer and the sample surface should be kept at about 30 cm, and the spray rate should be 0.25 L/min. Then, the sample surface was washed with deionized water.

$$Ni^{2+} + 4H_2PO_2^- + H_2O \rightarrow Ni + P + 3H_2PO_3^- + H^+ + \frac{3}{2}H_2 \uparrow \quad (1)$$

$$4NaH_2PO_2 \rightarrow Na_4P_2O_7 + 2PH_3 + H_2O \quad (2)$$

Table 2. Activation solution formulations.

Reagent	Concentration
$NiSO_4{\cdot}6H_2O$	10 g/L
$NaH_2PO_2{\cdot}H_2O$	60 g/L

High-efficiency non-destructive activation focused on using a high temperature to provide the energy required for chemical reactions. In the activation of this experiment, the heat source utilized the high-frequency changing magnetic field to generate eddy currents in the metal object. When eddy currents flowed inside the metal, heat was generated due to the high-speed friction of free electrons, thereby achieving the temperature rise

in the substrate [27,28]. The principle is shown in Figure 2. This heating method has the characteristics of high efficiency and fast heat transfer, making the sample reach the required temperature for reaction in an extremely short time. In the activation process of this experiment, there are many factors affecting the activation effect, among which the main influencing factors are the concentration of Ni^{2+} and $H_2PO_2^-$ ions and the heating temperature. Due to the high temperature required for the reaction and the fact that the activation solution will lower the surface temperature of the substrate during the activation spray process, the heating temperature of the substrate needs to be higher than the temperature required for the reaction in order to ensure the formation of nickel particles on the substrate surface. This experiment proposed a heating temperature of 300–400 °C.

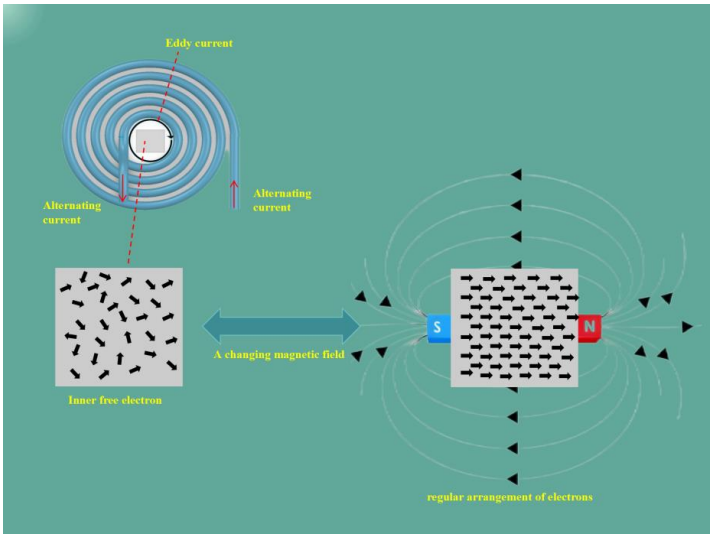

Figure 2. Electromagnetic induction heating principle schematic diagram.

From Equation (1), the ratio of Ni^{2+} to $H_2PO_2^-$ should be 1:4 under the condition of no loss, but, at high temperatures, sodium hypophosphite will be thermally decomposed into sodium pyrophosphate (Equation (2)), and the reduction in the amount of reducing agent in the reaction leads to a decrease in the reduction efficiency of nickel, so the concentration of $H_2PO_2^-$ should be higher than the required concentration in the reaction equation. If there is an excessive amount of sodium hypophosphite, it will decompose to generate sodium pyrophosphate attached to the surface of the substrate, affecting the attachment of nickel particles. Therefore, it was proposed to control the ratio of Ni^{2+} to $H_2PO_2^-$ by 1:6.

2.2.3. Nanoparticle Pre-Activation

For pre-activation treatment, Al_2O_3 nanoparticles (30 nm) were soaked in the activation solution for 10 min. Ultrasonic vibration and magnetic stirring devices were used to diffusely distribute nanoparticles in the activation solution. After carrying out solid–liquid separation using a high-speed tabletop centrifuge (TG16-WS), nanoparticles that had been soaked in the activation solution were placed in a box-type resistor furnace for heating. After a period of time, they were taken out and then put into the deionized water for ultrasonic cleaning. Finally, the solid–liquid separation was achieved by centrifuge and the solid obtained was dried in a 60 °C oven for later use.

2.3. Electroless Composite Plating Ni-P/Al_2O_3

There are many factors that affected the plating process, including the plating temperature, plating time and the amount of nanoparticle addition. The activated samples were soaked in the plating solution (as shown in Table 3), with a plating temperature of 85~95 °C, a time of 30~90 min and a nanoparticle addition of 1.5~2.5 g/L. The process was optimized according to the L9 (3^4) orthogonal experimental scheme, with the binding force and friction

coefficient of the composite coating as the evaluation indexes. According to the observation results, the evaluation indexes were rated from low to high as 1–10 points. The points of the two indexes were added together as the comprehensive score. The table of the orthogonal experiment is shown in Table 4 (the binding force score is based on GB/T9286-2021, and the abrasion resistance is based on the change of the friction coefficient).

Table 3. Plating solution formulation.

Reagent	Concentration
$NiSO_4 \cdot 6H_2O$	25~30 g/L
$NaH_2PO_2 \cdot H_2O$	20~40 g/L
$CH_3COONa \cdot 3H_2O$	10~20 g/L
$C_6H_5Na_3O_7 \cdot 2H_2O$	25~30 g/L
Al_2O_3 nanoparticle	1.5~2.5 g/L
$NiSO_4 \cdot 6H_2O$	25~30 g/L

Table 4. Factors and levels of orthogonal experiment.

Level	Factors A	Factors B	Factors C
	Time/min	Nanoparticle Addition/(g/L)	Temperature/°C
1	30	1.5	85
2	60	2	90
3	90	2.5	95

2.4. Method Description

The SDC-350H optical contact angle measuring instrument was used to test the water contact angle of the sample before and after activation, and the effect of oil removal was judged by the hydrophilicity and hydrophobicity of the sample. A digital thermometer (DM6801B) was used to measure the surface temperature of the sample. SEM was used to observe the surface morphology of the substrate before and after activation and composite coating. EDS was used to carry out energy spectral analysis of the activated layer and composite coatings. XPS was used to analyze the elemental state of the activated layer surface.

The hardness was calculated according to the Vickers hardness Formula (3):

$$HV = 0.102 \times (F/S) = 0.102 \times \left(2Fsin\frac{\alpha}{2}\right)/d^2 \quad (3)$$

F = load (N).

S = surface area of indentation (cm^2).

α = angle of the relative faces of indenter = 136°.

d = average indentation diagonal length (mm).

A thermal shock method (ASTMB571) was used to test the sample. The sample of electroless nickel plating composite coating obtained from the experiment was placed in a 200 °C oven, heated for 60 min and then put into the room-temperature water cooling. The step was repeated 5 times. The surface coating of the sample showed no cracking or peeling, indicating a good binding force of the coating. A scratch test (GB/T9286-2021) was carried out by using a cross-cut tester. A cross-cut tester was used to form a lattice pattern on the surface of the coating, and then the tape was used to test whether the coating was off. Under the microscope, if the lattice pattern was formed into a square arrangement and the coating was not peeling, cracking or falling off, then the binding force was in line with the standard.

A multifunctional friction and wear tester (MFT3000, RTEC, USA, Beijing Zhongjingyi Technology Co.) was used to carry out sliding friction tests on the substrate and the Ni-P layer and Ni-P/Al_2O_3 composite coating prepared under optimal technological conditions.

Because the application requirements of using titanium alloy parts are relatively high, the whole is generally made of titanium alloys, and the friction is usually the titanium alloy parts interacting with each other. So, for the friction vice selection of a 4 mm radius titanium alloy ball, Rtec Viewer (1.0.4.0) software for fitting friction wear experimental data, friction load 3 N, linear displacement 5 mm, friction time 30 min and sliding rate 2 mm/s was used.

The surface roughness of the applied substrate was examined using a white light interferometer and then the data were fitted using Lambda software to generate data and images.

3. Results and Discussion

3.1. Substrates before and after Degreasing

Figure 3a,b are the surface microscopic morphologies before and after the alkaline degreasing treatment. It can be clearly observed that the surface of the sample was clearer after degreasing, the surface lipids dissolved after degreasing treatment and the surface hydrophilicity was greatly improved. As shown in Figure 3c,d, the water contact angle decreased from the original 78.967° to 48.54°, and the effect of degreasing was obvious, so the substrate could make better contact with activated particles and provide a place for particle attachment.

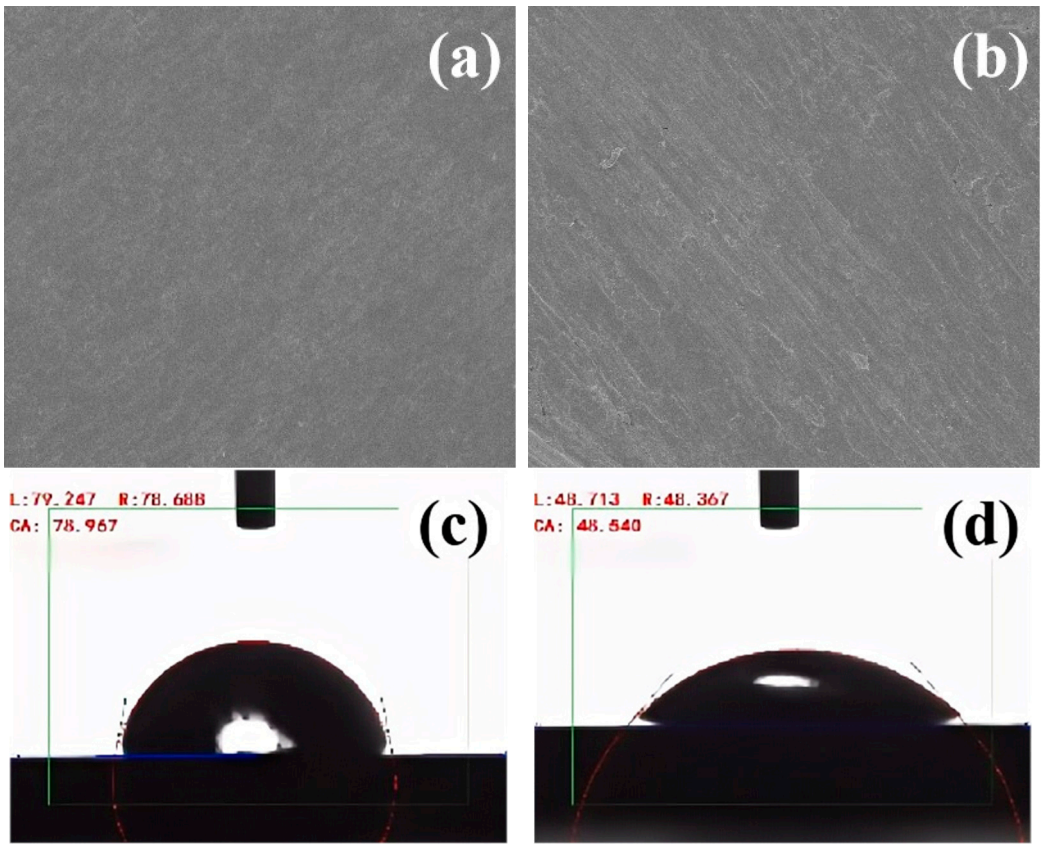

Figure 3. (**a**,**b**) SEM images of the surface before and after degreasing. (**c**,**d**) Images of water contact angle.

3.2. Activation Analysis

3.2.1. Activation Analysis of the Substrate

An electromagnetic induction heater was used to heat the titanium alloy, a digital thermometer was used to monitor the temperature change on the surface of the substrate and the temperature curve was measured over time, as shown in Figure 4. The figure shows that the time required from the beginning of heating until the temperature reached 300~400 °C was only 20~25 s. After leaving the heat source, the temperature dropped

rapidly within 35 s. Therefore, when the sample left the heat source, an atomizer was used to spray the activation solution onto the surface of the sample in order to ensure the success of the activation. The whole activation process takes less time, while the traditional method requires zinc dipping, which is a lot of steps and requires a huge amount of drugs. In contrast, this process is fast and efficient.

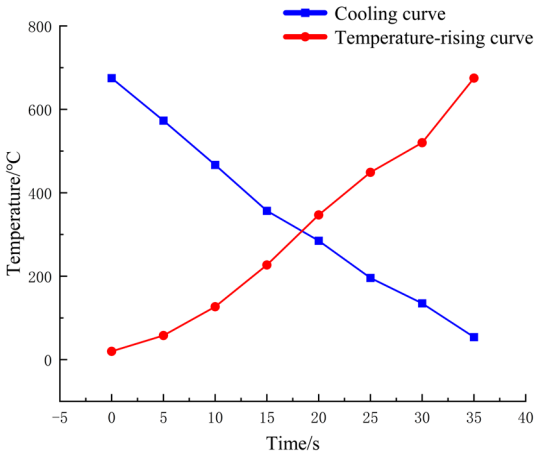

Figure 4. Temperature curve over time.

The surface of the sample after activation was analyzed by EDS, and as shown in Figure 5, the surface of the sample contained four elements: Ti, Ni, P and O. Figure 6 shows the XRD graph of the sample after activation. At 2θ about 44.5°, the diffraction peak of O appeared, and, analyzed by jade software, the peak oxide was TiO_2, and element O appeared because the oxide layer was not removed from the surface of the sample, which was in line with the inference. Ni was distributed on the surface of the specimen, and, at the same time, combined with the scanning data, it was demonstrated that the nickel particles attached to the surface of the specimen. The composition of the activated substrate surface was analyzed by XPS, as shown in Figure 7. The orbital peaks of Ni_{2p}, Ti_{2p}, P_{2p}, O_{1s} and C_{1s} appeared on the surface of the activated substrate, respectively, and there were two main peaks in the energy spectra at 852.8 eV and 870.4 eV, which corresponded to the energy levels of 2p3/2 and 2p1/2 of Ni, which indicated that there was metallic nickel attached to the surface of the activated substrate. Combined with Figure 5, it is shown that the new activation process can produce a layer of metallic nickel with catalytic activity on the surface of the substrate.

3.2.2. Pre-Activation Analysis of Nanoparticles

Al_2O_3 nanoparticles have the property of high temperature resistance, but prolonged exposure to high temperatures can lead to creep phenomenon [29], which can affect subsequent operations and the coating quality. If the heat treatment time is too short, the surface of the nanoparticles cannot reach the required temperature, so the activation effect is bad. During the heat treatment process on their surfaces, nanoparticles absorb and dissipate heat quickly. Therefore, after soaking in the activation solution, it is best to perform heat treatment for 2–3 min.

EDS was used to analyze activated nanoparticles. As shown in Figure 8, the element distribution map shows that the sample surface contained O, Al, P and Ni elements, and the distribution was consistent. Combined with scanning data, it was proven that there were nickel particles attached to the surface of the nanoparticles, and the activation of the nanoparticles was successful. To further verify the results, the treated nanoparticles were examined by XPS, and the results are shown in Figure 9. The orbital peaks of Ni2p, Al2p, P2p, O1s and C1s appeared on the surface of the activated nanoparticles, respectively, which indicates that the nanoparticles were activated successfully.

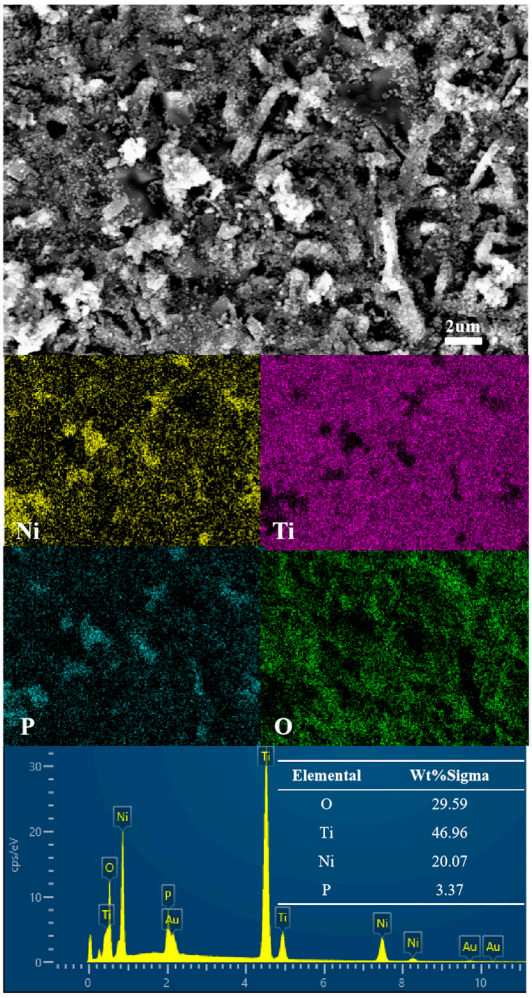

Figure 5. SEM and EDS of the surface of the activated sample.

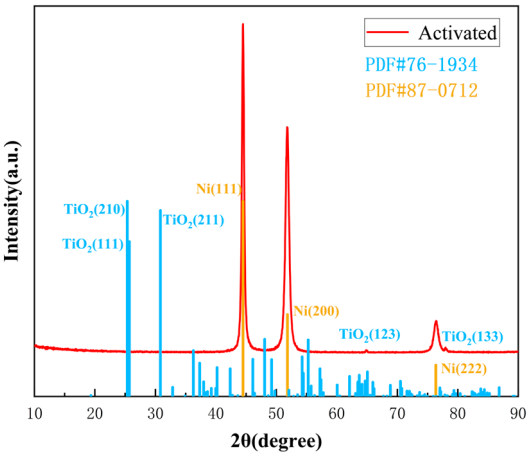

Figure 6. XRD of the surface after activation of the specimen.

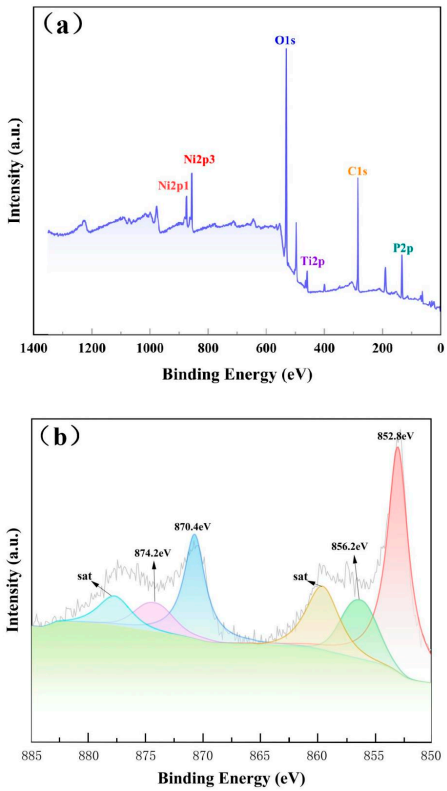

Figure 7. (**a**) Full spectrum of the activated sample surface; (**b**) Ni spectrum of the activated sample surface.

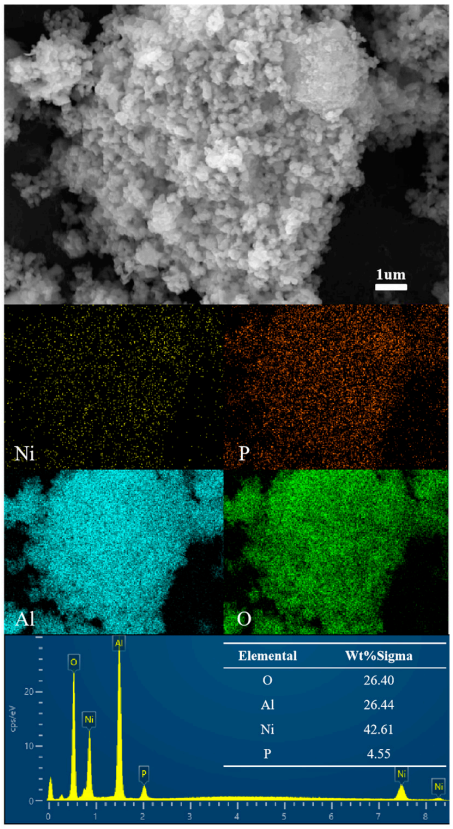

Figure 8. SEM and EDS of Al_2O_3 nanoparticles after activation.

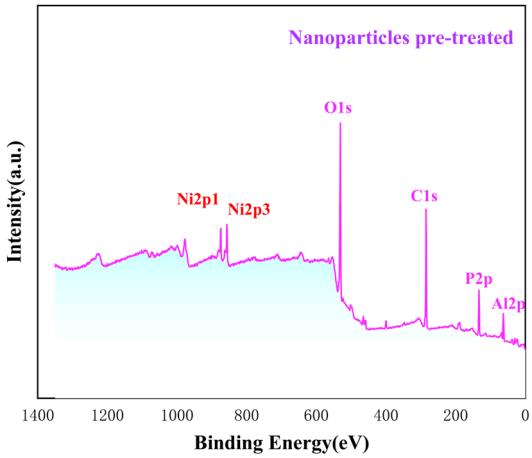

Figure 9. Full spectrum of nanoparticles after pre-activation.

3.3. Optimization of Composite Plating Process Parameters

In the composite plating process, there are many factors affecting the quality of the composite coating, among which plating time, plating temperature and nanoparticle additions have the greatest influence. The results of the L9 (3^4) orthogonal experiments and range analysis are shown in Table 5.

Table 5. Result and range analysis of orthogonal test.

Test No.	A	B	C	Bonding Score	Friction Factor Score	Aggregate Score
1	30	1.5	85	6.5	8	14.5
2	30	2	90	6.5	6.5	13
3	30	2.5	95	6.5	7	13.5
4	60	2	95	8.5	8	16.5
5	60	2.5	85	7.5	8	15.5
6	60	1.5	90	9	8.5	17.5
7	90	2.5	90	7.5	6.5	14
8	90	1.5	95	6	6.5	12.5
9	90	2	85	6	6	12
Average value 1	13.67	15.00	14.83			
Average value 2	16.50	13.67	13.83			
Average value 3	12.83	14.33	14.16			
Extremely poor	3.67	1.33	1.00			

According to the experimental results, the degree of influence of the three factors on electroless composite plating is ranked as follows: A > B > C.

The effect of plating time on the electroless composite plating. After a certain time of deposition of metal ions in the plating solution, the thickness of the coating thickened with the increase in plating time. If the plating time was too short, the thickness of the coating did not meet the standard and had poor surface continuity. If the plating time was too long, it led to a decrease in ionic concentration, and the reaction was weak or even did not react, which consumed a lot of energy. Therefore, it needed to be strictly controlled by the time of the plating in the plating process. Under the conditions of the experiments, the optimum plating time was 60 min.

The effect of the nanoparticle concentration on the electroless composite plating. In the experimental process, the plating rate increased as the concentration of nanoparticle increased. When the nanoparticle concentration reached a certain level, the plating rate decreased accordingly, as shown in Figure 10. Regarding the mechanism, a certain amount of nanoparticles was added to the plating solution. They were deposited with Ni-P on the surface of the sample, thereby increasing the surface area of autocatalysis. When the

nanoparticle concentration was saturated, the non-conductive nanoparticles were prone to agglomeration [30], which masked some catalytic active points and they lost their effectiveness, and the plating rate slowed down, so the optimal amount of nanoparticle addition was 1.5 g/L.

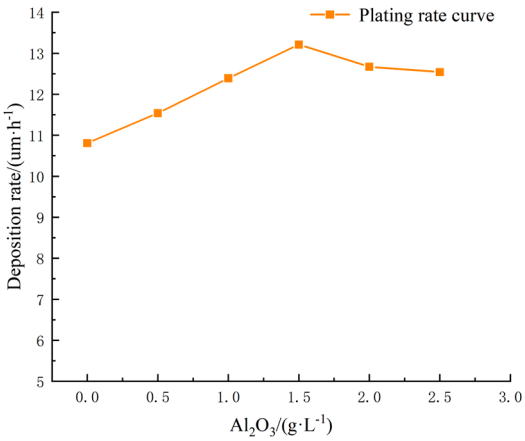

Figure 10. Effect of Al_2O_3 nanoparticles on deposition rate.

The effect of temperature on electroless composite plating. Temperature can provide energy for the reaction, making more molecules more active so that the molecules attach to the surface of the sample faster and the rate of reaction speeds up. The optimal temperature obtained from the experiment was 85 °C.

In summary, the optimal combination of this experiment was $A_2B_1C_1$, with the plating time of 60 min, the nanoparticle addition of 1.5 g/L and the plating temperature of 85 °C.

3.4. The Analysis of the Composite Coating

The surface morphology and constituent elements of the samples prepared under the optimal process were analyzed by SEM and EDS. As shown in Figure 11, the coating surface contained four elements: Al, Ni, P and O. The elemental distribution map shows that Ni, Al and O were uniformly distributed on the surface of the samples. The scan data were combined and Figure 12 shows that the Al_2O_3 nanoparticles uniformly dispersed on the surface of the sample along with the nickel grains, which corroborated the successful addition of the nanoparticles.

The cross-section of the coating prepared under the optimal process is shown in Figure 13a. The coating was tightly bonded to the substrate with uniform thickness, good conformality and a thickness of 12 μm. To test the binding force of the coating, thermal shock experiments were conducted on the coating prepared under the optimal process conditions. The coating surface showed no cracking or peeling after the thermal shock experiments.

A cross-cut tester was used for scratch experiments. The sample was placed on a flat plate and the cross-cut tester was perpendicular to the sample plane. The instrument was then used to cut at a uniform pressure and stable cutting speed. Next, the sample was rotated by 90° and the above operation was repeated to form the lattice pattern, as shown in Figure 13b. The figure shows that the coating coverage was completely covered, and no peeling of the coating was found at the cut and cross, indicating that the coating prepared was of good adhesion. According to the GB/T9286-2021 standard for the evaluation of the sample adhesion, the binding level of the sample was 0, while the coating prepared by traditional zinc dipping method showed a peeling phenomenon in the scratch test, as shown in Figure 13c.

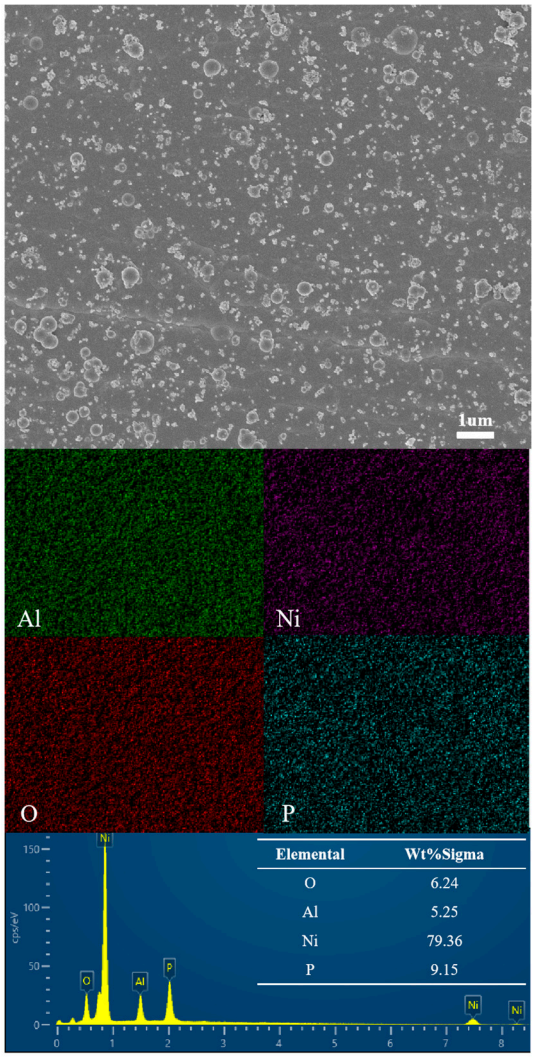

Figure 11. SEM and EDS of Ni-P/Al_2O_3 composite coating surface.

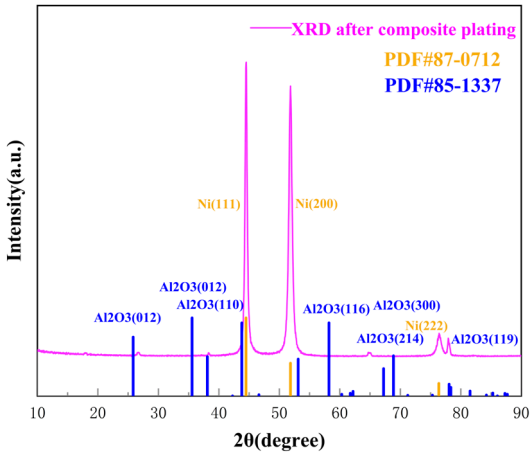

Figure 12. XRD image of the substrate after composite plating.

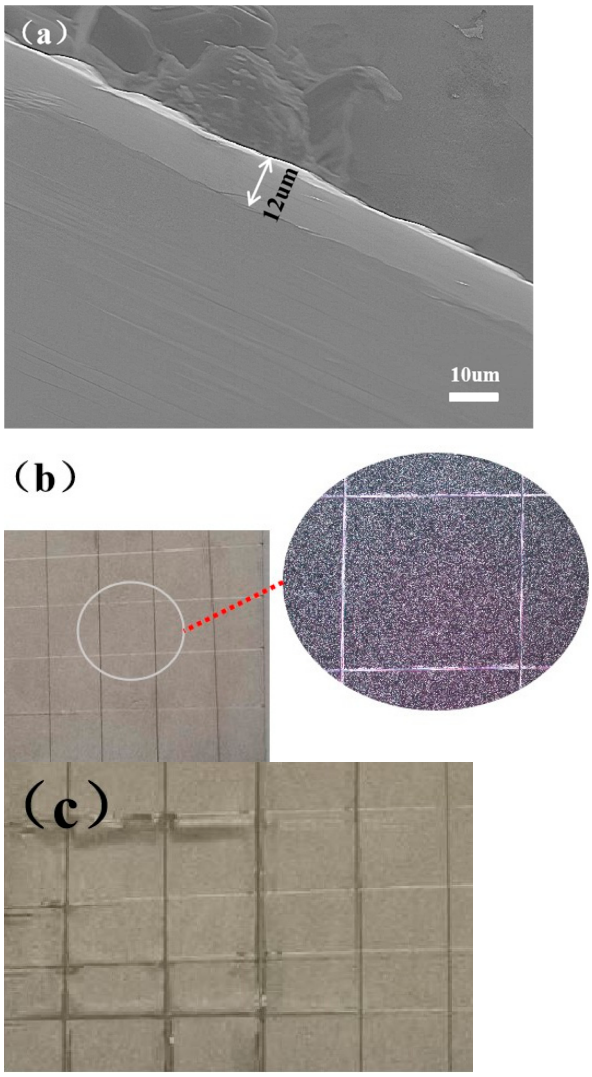

Figure 13. (**a**) SEM cross-section of composite plating; (**b**) coating scratch diagram of new process; (**c**) coating scratch diagram of zinc dipping.

A digital microhardness tester was used to perform an indentation process on the sample surface and a light microscope was used to observe the measured indentation and measure the diagonal length of each indentation. Then, the surface hardness was obtained through Formula (3). The results are shown in Table 6. Comparing testing results of the hardness, the microhardness of the substrate surface was 200.1 ± 0.5 HV_{500gf} and the surface hardness of the Ni/Al_2O_3 composite coating by electroless plating was increased to 688.5 ± 0.5 HV_{500gf}, while the surface hardness of the sample prepared by the traditional process was only 593.7 ± 0.5 HV_{500gf}. It shows that the surface hardness of the sample prepared by the new process was significantly improved compared with the traditional process. The main reason for the improvement of hardness was that the hard particle phase Al_2O_3 nanoparticles themselves had extremely high hardness. From the analysis of Figure 12, it can be seen that Al_2O_3 nanoparticles deposited on the substrate surface to form a composite coating, and were embedded in the coating, which played the role of dispersion reinforcement. As one of the main components of the coating, the performance of Al_2O_3 nanoparticles reacted to the coating at the same time, so the hardness of the composite coating was improved.

Table 6. Results of Vickers hardness test.

Samples	Untreated (xHV_{500gf})	Ni/Al_2O_3 Composite Layer (xHV_{500gf})
Point1	213.8 ± 0.5	680.6 ± 0.5
Point2	203.0 ± 0.5	691.8 ± 0.5
Point3	197.6 ± 0.5	709.7 ± 0.5
Point4	192.4 ± 0.5	671.1 ± 0.5
Point5	193.7 ± 0.5	689.5 ± 0.5
Average value	200.1 ± 0.5	688.5 ± 0.5

Rtec Viewer (1.0.4.0) software was used to fit the friction and wear experimental data, and compare friction coefficients. Figure 14a shows that the friction coefficient of the titanium alloy substrate surface was around 0.45 ± 0.05 in the friction and wear experiments. Under the optimal process conditions, the friction coefficient of the electroless nickel plating layer was around 0.35 ± 0.05, and the friction coefficient of the electroless Ni-P/Al_2O_3 composite plating layer was around 0.2 ± 0.05. This further demonstrates that electroless composite plating can enhance the surface wear resistance of the material, thereby enhancing the life span of the material in a frictional wear environment.

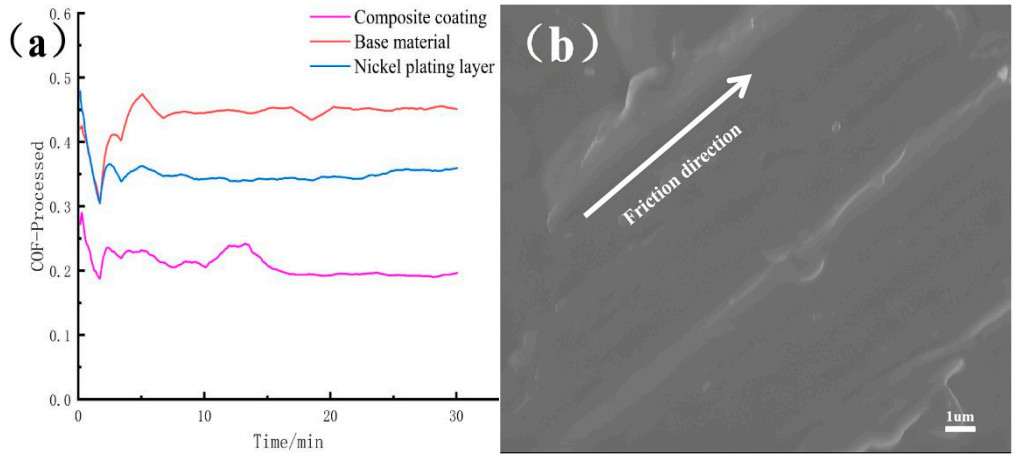

Figure 14. Variation curves of surface friction coefficient (**a**) and wear morphology (**b**) of titanium alloy substrate and its electroless Ni-P/Al_2O_3 composite plating.

SEM was used to observe the wear surface of the sample. As shown in Figure 14b, the abrasion marks on the wear surface were mainly typical parallel furrows, indicating that the main mechanism of sample wear was abrasive wear. The figure shows that the surface abrasion marks were shallow and did not damage the substrate. Some particles were scattered on the abraded surface, which should be the Al_2O_3 nanoparticles embedded on the surface of the coating during the abrasion process. The addition of nanoparticles increased the hardness of the coating, and the anti-abrasion performance was greatly improved. At the same time, the scattered nanoparticles also indicated that the nanoparticles reduced the friction by changing the friction form, i.e., sliding friction to composite friction of sliding and rolling, thus improving the wear resistance of the composite coating.

The roughness of the material surface also had some influence on the wear resistance of the substrate, as seen in Figure 15. The roughness was kept between 11.52 μm and 12.29 μm, and the change in roughness was relatively small, which indicated that the coating prepared by this method was relatively smooth.

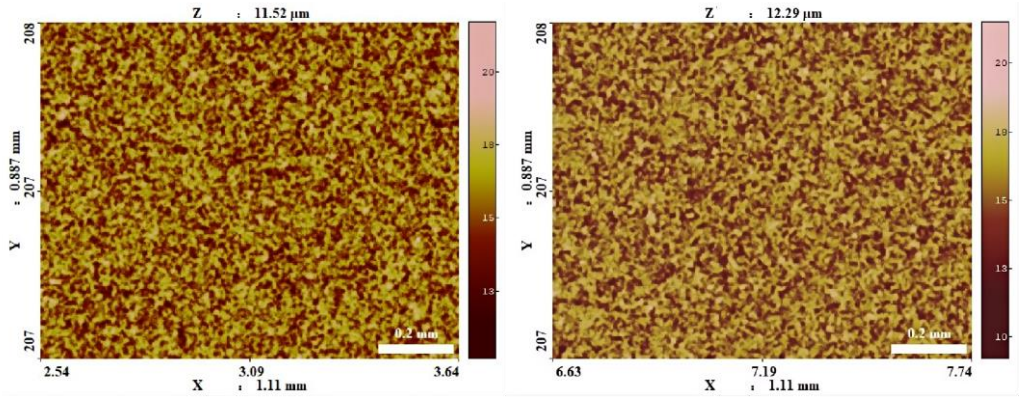

Figure 15. Scan of surface roughness after composite plating.

4. Conclusions

In this study, a new high efficient and non-destructive metal activation process of composite plating of Ni-P-Al_2O_3 on a titanium base and its wear resistance were proposed. For the activation of the titanium alloy in chemical composite plating, this process avoided the use of strong corrosive drugs to damage the surface of the material. At the same time, it enabled the metal to quickly reach the temperature required for the activation reaction and made the nickel nanoparticles uniformly adhere to the material surface. Also, attached nickel particles were used as reaction sites to form a uniform, dense and strong binding composite coating during the plating process. The appropriate addition of pre-activated nanoparticles could improve the binding force between the nanoparticles and the coating, and provide more space for the formation of nickel particles, thereby improving the plating rate. The plating rate under the optimal process could reach 12 μm/h.

The average Vickers hardness of the coating surface was increased from 200.1 ± 0.5 HV_{500gf} before the plating to 688.5 ± 0.5 HV_{500gf} after the plating. The wear resistance of the sample was tested by friction and abrasion testers, and the results showed that the friction coefficient of the titanium alloy substrate surface was around 0.45 ± 0.05. Under the optimal process conditions, the friction coefficient of the chemical nickel coating was around 0.35 ± 0.05 and the friction coefficient of the chemical Ni-P/Al_2O_3 composite coating was around 0.2 ± 0.05. The results indicate that the electroless Ni-P/Al_2O_3 composite coating has excellent wear resistance. This work provides effective ideas for improving the application value of titanium alloys in friction and wear environments. In conclusion, this study presents a new high efficient and non-destructive metal activation process, which is not only simple to operate, has a low cost and is environmentally friendly but also produces composite coatings with good performance. Therefore, the process has significant industrial potential.

Author Contributions: Conceptualization, J.G., K.C. and S.L.; methodology, J.G. and K.C.; validation, S.L., R.Q. and K.C.; formal analysis, L.Z. and X.L.; investigation, J.G. and S.L.; data curation, J.G. and S.L.; writing—original draft preparation, J.G. and S.L.; writing—review and editing, J.G., S.L. and K.C.; visualization, J.G., R.Q. and S.L.; supervision, L.Z., X.L. and K.C.; project administration, R.Q. and K.C.; funding acquisition, L.Z., J.G. and S.L. All authors have read and agreed to the published version of the manuscript.

Funding: This work was supported by the Science and Technology Department of Sichuan Province, China [grant number 23ZS2127]; the Science and Technology Department of Sichuan Province, China [grant number 20ZS2112]; the Sichuan Science and Technology Innovation Talent Project, China [grant number 2022JDRC0028]; the Research Foundation of Southwest University of Science and Technology, China [grant number 19zx7165].

Institutional Review Board Statement: Not applicable.

Informed Consent Statement: Not applicable.

Data Availability Statement: Data are contained within the article.

Conflicts of Interest: The authors declare no conflicts of interest.

References

1. Wang, B.; Hou, J.; Luan, J.; Xu, D.; Sun, H.; Sun, J. The Corrosion Behaviors of an As-Rolled Mg-8Li (in wt.%) Alloy in Two Differently Concentrated NaCl Solutions. *Coatings* **2022**, *12*, 406. [CrossRef]
2. Zhong, W.; Yu, K.; Shi, J.; Shen, Y.; Li, P.; Lu, J. High-temperature oxidation behavior of TA15 aerospace titanium alloy at 500 °C and 800 °C. *J. Mater. Res. Technol.* **2024**, *30*, 3355–3366. [CrossRef]
3. Song, W.W.; Feng, C.; Zhu, L.J.; Zhang, F.F. Progress of Laser Cladding Wear Resistant Coating on Titanium Alloy Surface: A Review. *Mater. Sci. Forum* **2021**, *6114*, 521–527. [CrossRef]
4. Cui, Y.; Liu, D.; Zhang, Y.; Deng, G.; Fan, M.; Chen, D.; Sun, L.; Zhang, Z. The Microstructure and Mechanical Properties of TA1-Low Alloy Steel Composite Plate Manufactured by Explosive Welding. *Metals* **2020**, *10*, 663. [CrossRef]
5. Huang, P.; Zou, B.; Zhang, Y.; Niu, X.; Wang, Y. Synthesis of rare earth silicate thermal barrier coating materials ($Y_xYb_{2-x}SiO_5$) and application on the surface of titanium alloy. *Inorg. Chem. Commun.* **2022**, *135*, 109129. [CrossRef]
6. Jingshuang, Z.; Zhelong, Y.; Maozhong, A.; Zhenmi, T.; Mengchu, L. A New Process of Electroplating on Titanium and Titanium Alloy for Aerospace. *Trans. IMF* **2017**, *74*, 25–27. [CrossRef]
7. Banjo, N.; Sasaki, T.; Hono, K. Microstructure control of Ti-based conversion coatings for optimizing organic coating properties in A6063 and A3003 alloys. *Surf. Coat. Technol.* **2023**, *468*, 129735. [CrossRef]
8. Zheng, H.; Yin, Y.; Li, R.; Liu, C.; Chen, Q. Preparation and properties of FeS/iron-based self-lubricating materials by chemical nickel plating-mechanical alloying. *Ind. Lubr. Tribol.* **2024**, *76*, 658–665. [CrossRef]
9. Vaibhav, N.; Satyajit, C. Evaluation of microstructural, mechanical, and tribological characteristics of Ni-B-W-SiC electroless composite coatings involving multi-pass scratch test. *J. Mater. Charact.* **2021**, *180*, 111414. [CrossRef]
10. Boschloo, K.G.; Goossens, A.; Schoonman, J. Photoelectrochemical Study of Thin AnataseTiO_2 Films Prepared by Metallorganic Chemical Vapor Deposition. *J. Electrochem. Soc.* **2019**, *144*, 1311–1317. [CrossRef]
11. Chen, J.; Guo, Q.; Yang, Z.; Li, J.; Guo, Y.; Yang, W.; Xu, D. Effects of Micro-arc Oxidation/Multi-arc Ion Plating Composite Treatment on Microstructure and Properties of TC4 Titanium Alloy. *J. Mater. Eng. Perform.* **2023**, *33*, 1391–1400. [CrossRef]
12. Kowalski, S.; Gonciarz, W.; Belka, R.; Góral, A.; Chmiela, M.; Lechowicz, Ł.; Kaca, W.; Żórawski, W. Plasma-Sprayed Hydroxyapatite Coatings and Their Biological Properties. *Coatings* **2022**, *12*, 1317. [CrossRef]
13. Vlcak, P.; Fojt, J.; Koller, J.; Drahokoupil, J.; Smola, V. Surface pre-treatments of Ti-Nb-Zr-Ta beta titanium alloy: The effect of chemical, electrochemical and ion sputter etching on morphology, residual stress, corrosion stability and the MG-63 cell response. *Results Phys.* **2021**, *28*, 104613. [CrossRef]
14. Wei, X.C.; Wang, J.B.; Zhang, X.M.; Wang, X.G. Study on the Development of Pretreatment Processes of Electroless Nickel Plating on Al Alloy Surface. *Mater. Sci. Forum* **2014**, *809–810*, 412–418. [CrossRef]
15. Shao, Z.; Zhang, F.; Cai, Z.; Hu, R. Process and performance of electroless nickel plating on AZ91D magnesium alloy. *Anti-Corros. Methods Mater.* **2017**, *64*, 162–169. [CrossRef]
16. Allahkaram, S.R.; Salmi, S.; Tohidlou, E. An investigation on effects of tio2 nano-particles incorporated in electroless nip coatings' properties. *Int. J. Mod. Phys. Conf. Ser.* **2012**, *5*, 833–840. [CrossRef]
17. Su, W. Microhardness of Electroless Composite Coating of Ni-P with SiC Nano-Particles. *Adv. Mater. Res.* **2013**, *2290*, 223–226. [CrossRef]
18. Dang, X.; Cui, K.; Zhuang, J.; Zhong, L.; He, Y.; Li, G.; Du, G.; Yang, Z.; Pei, S.; Li, S. A new process for environmentally friendly and non-destructive activation of electroless nickel plating on alumina ceramics. *Mater. Today Commun.* **2023**, *35*, 105506. [CrossRef]
19. Ma, H.; Feng, Y.; Li, N.; Tan, C.; Zhang, L. Effect of MoS_2 nanoparticles on the properties of Ni-W-SiC composite coatings. *Int. J. Electrochem. Sci.* **2024**, *19*, 100654. [CrossRef]
20. Jia, Y.; Lai, J.; Yu, J.; Qi, H.; Zhang, Y.; He, H. Tribological Behaviors of Electroless Nickel-Boron Coating on Titanium Alloy Surface. *Chin. J. Mech. Eng.* **2024**, *37*, 13. [CrossRef]
21. Cao, J.; Zhao, W.; Wang, X.; Zhao, Y.; Ma, P.; Jiang, W.; Song, G. The Microstructure and Tribological Behavior of Ultrasonic Electroless Ni-P Plating on TC4 Titanium Alloy with Heat-Treatment. *Ferroelectrics* **2022**, *589*, 1–11. [CrossRef]
22. CCui, C.; Gu, A.; Xiao, M.; Xu, L.; Li, H.; Yang, Z.; Dong, T.; Gao, H.; Jiang, F. A novel in-situ activation method on titanium alloys for electroless plating. *Mater. Lett.* **2020**, *276*, 128275. [CrossRef]
23. Che, L.; Xiao, M.; Xu, H.; Wang, B.; Jin, Y. Enhanced Corrosion Resistance and Microhardness of Titanium with Electroless Deposition Ni-W-Cr-P Coating. *Mater. Manuf. Process.* **2013**, *28*, 899–904. [CrossRef]
24. Yang, Z.D.; Wu, D.; Liu, M.F. Electroless Ni-P-PTFE Composite Coatings on Titanium Alloy and Their Tribological Properties. *Adv. Mater. Res.* **2011**, *1335*, 12–17. [CrossRef]
25. Rani, R.U.; Sharma, A.K.; Minu, C.; Poornima, G.; Tejaswi, S. Studies on black electroless nickel coatings on titanium alloys for spacecraft thermal control applications. *J. Appl. Electrochem.* **2010**, *40*, 333–339. [CrossRef]
26. Khalid, A.R.; Khammas, H.A.; Kais, A.L. Enhanced alumina substrate wear resistance via electroless NiP–TiC nanocomposite coating. *Results Mater.* **2023**, *20*, 100466. [CrossRef]
27. Xu, J.; Gu, Y.; Fu, T.; Zhang, X.; Zhang, H. Research on the Heating Process of CFRP Circular Tubes Based on Electromagnetic Induction Heating Method. *Polymers* **2023**, *15*, 3039. [CrossRef]

28. Cervera-Gabalda, L.; Gómez-Polo, C. Magnetic carbon Fe_3O_4 nanocomposites synthesized via Magnetic Induction Heating. *Sci. Rep.* **2023**, *13*, 7244. [CrossRef]
29. Harada, Y.; Suzuki, T.; Hirano, K.; Nakagawa, N.; Waku, Y. Creep Behaviors of In-Situ Single-Crystal Al_2O_3/YAG and Al_2O_3/GAP Eutectic Composites. *J. Ceram. Soc. Jpn.* **2004**, *112*, S294–S298. [CrossRef]
30. Castillo-Rodríguez, M.; Muñoz, A.; Domínguez-Rodríguez, A. Creep study on Alumina and Alumina/SWCNT nanocomposites. *J. Eur. Ceram. Soc.* **2018**, *38*, 5497–5502. [CrossRef]